

## Measurements of Wave-Breaking Radiation from a Laser-Wakefield Accelerator

A. G. R. Thomas,<sup>1</sup> S. P. D. Mangles,<sup>1</sup> Z. Najmudin,<sup>1</sup> M. C. Kaluza,<sup>1,\*</sup> C. D. Murphy,<sup>1,2</sup> and K. Krushelnick<sup>1</sup>

<sup>1</sup>*Blackett Laboratory, Imperial College London, SW7 2AZ, United Kingdom*

<sup>2</sup>*Central Laser Facility, Rutherford Appleton Laboratory, Chilton, Oxon, OX11 0QX, United Kingdom*

(Received 8 September 2006; published 2 February 2007)

Spectral analysis of radiation emitted transverse to laser propagation in laser-wakefield acceleration experiments shows broadband emission when electrons are accelerated to relativistic energies. The region over which emission occurs is short compared with the overall interaction length. The energy of the emission and location along the interaction length both vary with plasma density. A model for the radiation from self-trapped electrons indicates that the emission is a signature of the violent initial acceleration, and hence can be used as a diagnostic of the self-injection mechanism.

DOI: [10.1103/PhysRevLett.98.054802](https://doi.org/10.1103/PhysRevLett.98.054802)

PACS numbers: 41.75.Jv, 41.60.-m, 41.75.Ht

The production of monoenergetic electron beams from intense laser-plasma interactions has been recently demonstrated using the Laser-Wakefield Accelerator (LWFA) scheme [1–3]. An ultraintense ( $>10^{18}$  W cm<sup>-2</sup>) laser pulse propagates through an underdense plasma, ponderomotively displacing electrons. The displacement sets up a charge separation with the ions, which are stationary on the time scale of the laser pulse ( $\sim 50$  fs). The electrons then oscillate as a plasma wave with a phase velocity close to the group velocity of the pulse [4]. Relativistic electrons can stay in phase with the longitudinal accelerating electric field of this plasma wakefield, and therefore gain very high energies. If the laser pulse is sufficiently intense, then trapping of electrons can occur from the background plasma [5–10].

The pulse durations and energies of current laser systems are such that, in general, self-focusing and compression of the pulse are required before the onset of electron trapping. The time at which trapping occurs in the interaction is critical to the stability of the resultant electron beam, particularly in energy. Diagnosing the self-injection process would therefore be a useful tool for research into wakefield acceleration, particularly for high power laser systems in development.

When injection occurs, a large bunch ( $\sim 10^8$ – $10^9$ ) [1,2] of electrons experiences a violent change in velocity over a short period of time from a small volume ( $\ll \lambda_p^3$ ). This leads to a rapidly changing current and therefore radiation emission. The short time scale of the acceleration implies that the associated radiation spectrum is broadband. This radiation signature of injection will be detectable in the direction transverse to the acceleration direction, and can be used to precisely measure where injection occurs during the interaction.

In this Letter, we present experimental observation of spatially localized broadband radiation emission in the direction perpendicular to the laser propagation direction. This emission is shown to be correlated with the production of beams of relativistic electrons. A model for the generation of transversely emitted radiation from the electrons accelerated by the wakefield is also developed. The

model suggests that the broadband emission is due to the injection and violent acceleration of plasma electrons, and hence that this process can be used as a diagnostic of the self-injection mechanism.

The laser-wakefield acceleration experiments were carried out on the Ti:sapphire ASTRA laser at the Rutherford Appleton Laboratory, which provides pulses of energy up to  $E_L = 500$  mJ, pulse duration  $\tau = 40(\pm 5)$  fs FWHM at a center wavelength  $\lambda_0 = 800$  nm. The laser was focused with an  $f/16$  off-axis parabolic mirror, where the  $f$  number refers to the ratio of focal length to initial beam diameter. The measured spot-size (FWHM) at focus was  $25 \mu\text{m}$  ( $1.3 \times$  diffraction limit), and the normalized peak vector potential in vacuum  $a_0 = eA/m_e c \approx 1$ . The pulse was focused onto the front edge of a 2 mm diameter supersonic helium gas jet. This provided initial electron densities of  $4 \times 10^{18} \text{ cm}^{-3} < n_e < 4 \times 10^{19} \text{ cm}^{-3}$ .

The energy spectrum of the accelerated electrons was measured with a magnetic spectrometer using image plate detectors. In addition, a LANEX screen behind a metal filter provided divergence measurements of the relativistic electrons ( $\geq 5$  MeV). However, these two measurements could not be performed simultaneously. Light scattered at  $90^\circ$  to the direction of propagation was reimaged both perpendicular (top view) and parallel (side view) to the laser polarization plane. The image in the top view was also spectrally dispersed perpendicular to the channel direction, which gave the spectrum of scattered light along the channel length.

The electron energies measured over this density range typically consisted of peaked spectra, but did not always have a single monoenergetic spike, although such spectra frequently occurred. The measured electron spectra (Fig. 1) varied in charge and energy from shot to shot. However, beam divergence measurements taken separately indicated that electron beams were consistently produced for  $n_e \geq 1 \times 10^{19} \text{ cm}^{-3}$ . These took the form of one or more well collimated beamlets, with the collimation increasing for decreasing density.

Figure 2 shows an example of simultaneous measurements of radiation emission in the two orthogonal direc-

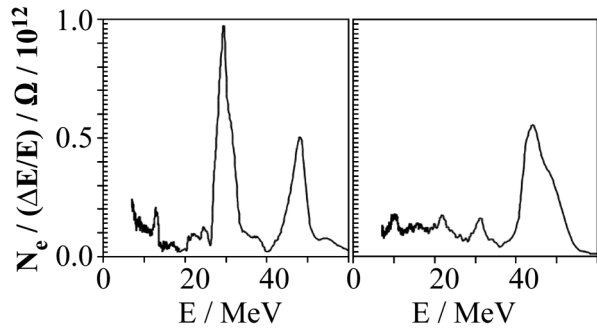


FIG. 1. Typical electron energy spectra measured on the experiment for  $n_e = 1 \times 10^{19} \text{ cm}^{-3}$ .

tions transverse to the laser propagation. In addition, the spatially resolved spectrum is also shown; Fig. 2(c) shows the same emitted radiation as (a) radially integrated and dispersed spectrally in the vertical (transverse) direction.

The imaging channels (a) and (b) were generally characterized by  $\sim 200\text{--}500 \mu\text{m}$  of bright radiation, which is redshifted with respect to  $\lambda_0$  (labeled  $\beta$ ). The separation of this feature relative to  $\lambda_0$ , as a function of density, is consistent with a Raman process. Although the pulse duration is extremely short for growth of side-scattered Raman instabilities, the pulse near-field is not Gaussian but is clipped by an aperture. This contributes to transverse  $\mathbf{k}$  vectors in the pulse which increase amplification of side-scatter [11]. The second harmonic of this scatter (labeled  $\alpha$ ) is also evident. This initial bright emission is indicative of a period over which an initially long pulse ( $c\tau \gtrsim \lambda_p$ ) evolves to a shorter, more intense pulse through the combined action of self-focusing, self-compression and photon deceleration [10,12–14].

With the spectrometer filtering level dramatically reduced, a cascade of up-shifted Raman-like satellites equally spaced in frequency are also evident. However,

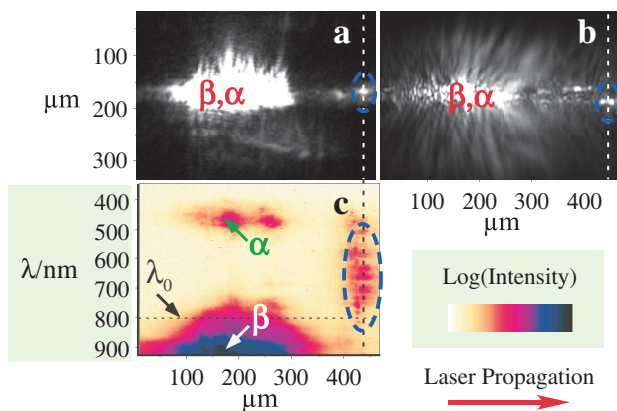


FIG. 2 (color online). Simultaneous measurement of (a) top view image (b) side view image (with  $800 \pm 20 \text{ nm}$  interference filter) and (c) imaging spectrometer for a shot at  $3.2 \times 10^{19} \text{ cm}^{-3}$ . The laser propagates from left to right.  $\alpha$  and  $\beta$  are the Stokes line of Raman side-scatter and its associated second harmonic. Circled is emission of broadband radiation occurring later in the interaction.

their separation is not exactly  $\omega_p$  but closer to  $3\omega_p/2$ . The satellites at higher frequency than the laser fundamental are of extremely low amplitude compared with the lower frequency satellite in the figure, as up-shifting is nonresonant for side scatter [15] and must rely on high-order wave mixing processes. Scattering at the laser frequency is also evident due to incoherent Thomson scattering, but this is also of extremely low intensity.

Also visible at the end of the channel, after a short dim region, is radiation emission in both transverse directions that is measured to be broadband in character, as Fig. 2(c) shows. The emission is of length  $\sim 30 \mu\text{m}$ . Since the pulse travels at  $\approx c$  and is short compared to these features, this spatial scale corresponds to an emission time of  $\sim 100 \text{ fs}$ . The total energy over the spectral range of Fig. 2 is  $\sim 10^{-10} \text{ J}$ , collected in an  $f/6$  cone. This emission is observed only for densities where electrons are produced, and is correlated to the charge in the bunch. At the higher densities, multiple longitudinal (and therefore temporal) incidences of the emission can occur, which correspond to the multiple electron beamlets that are often observed on the divergence diagnostic.

Figure 3 shows how the energy of the broadband radiation varies with initial electron number density  $n_e$ . There is an increase in radiated energy with  $n_e$ , which is consistent with an increase in trapped electron density. The right-hand side of the figure also shows that the position of the earliest peak follows an inverse relationship with  $n_e$ , suggesting a quicker evolution of the laser at higher density. At the lowest plasma densities ( $n_e \leq 1 \times 10^{19} \text{ cm}^{-3}$ ) no high-energy electrons were detected in the forward direction, and the broadband emission was also absent. These observations all suggest that the violent acceleration of electrons during self-injection is responsible for the radiation generated.

The rapid acceleration of forward going electrons results in a transverse emission of radiation with power proportional to  $\dot{v}^2$ . The radiated energy  $E$  as a function of spectrum is given by [16]:

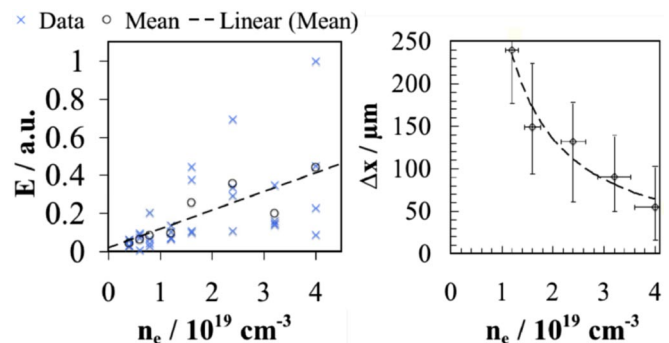


FIG. 3 (color online). (Left) The total energy  $E$  in the broadband radiation emission as a function of initial electron number density  $n_e$  with a linear fit. (Right) The relative position  $\Delta x$  from focus of the earliest emission as a function of  $n_e$  with  $1/n_e$  fit.

$$\frac{d^2 E}{d\Omega d\omega} = \frac{\omega^2}{4\pi^2 c^3} |\hat{\mathbf{s}} \times \mathbf{j}(\mathbf{k}, \omega)|^2, \quad (1)$$

where  $\mathbf{j}(\mathbf{k}, \omega)$  is the integral Fourier transform of the current density function  $\mathbf{j}(\mathbf{r}, t)$  and  $\hat{\mathbf{s}}$  is the observation direction. For an electron bunch of  $N$  particles in the wave frame coordinates,  $\mathbf{r} = (\xi = z - v_{\text{ph}} t, x, y)$ ,  $\tau = t$ , where  $v_{\text{ph}}$  is the phase velocity of the wake, the current density can be written as

$$\mathbf{j}(\mathbf{r}, \tau) = -|e| \sum_N v_N(\tau) \delta(\xi - \xi_N(\tau)), \quad (2)$$

where  $\delta(\xi - \xi_N(\tau))$  is a Dirac delta function, and  $\xi_N$  denotes the position of the  $N$ th particle.  $\tilde{\omega} = \omega + k v_{\text{ph}}$  is equivalent to the conjugate variable of  $\tau$  in the snapshot coordinate system  $\xi = z - v_{\text{ph}} t$ ,  $t = \tau$  [17], whereas  $k$  is the conjugate variable of  $\xi$ . The Fourier transform of Eq. (2) can be written in terms of the convolution of the two terms for  $v_N(\tau)$  and space  $\delta(\xi - \xi_N(\tau))$ . But from Fourier theory the transform of the velocity can be written in terms of the transform of the acceleration  $dv_N(\tau)/d\tau$ ;  $\dot{v}_N(\omega) = i\omega v_N(\omega)$ .

To model the acceleration function  $\dot{v}_N(\omega)$ , a sharp impulse at a time  $\tau_N$  for each electron is assumed. This is consistent with trapped electrons, which must be accelerated to  $\sim c$  very rapidly to stay in phase with the accelerating potential of the wakefield. Subsequently, even though the electron momentum increases dramatically, the acceleration is effectively zero. In the one-dimensional case this is accurate as when the wave steepens at wave breaking, the velocity of the electron changes from 0 to  $v_{\text{ph}}$  in  $\ll 1/\omega_p$ . In three dimensions the situation is more complex, but the electrons must still be accelerated to  $v_{\text{ph}}$  over a short distance to be trapped.

A Dirac delta function will therefore be used to describe the acceleration. In addition, it is assumed that the wake phase  $\mathbf{r}_N$  where the trapping occurs has no  $\tau$  dependence. This simplifies the Fourier transforms so that the current can be expressed as simply

$$\mathbf{j}(\mathbf{k}, \tilde{\omega}) = -\frac{|e|}{\tilde{\omega}} g(\mathbf{k}, \tilde{\omega}), \quad (3)$$

where  $g(\mathbf{k}, \tilde{\omega})$  is the Fourier transform of  $g(\mathbf{r}, \tau) = \sum_N \delta(\tau - \tau_N) \delta(\mathbf{r} - \mathbf{r}_N)$ . Hence the spectral energy in the direction transverse to the motion becomes

$$\frac{d^2 E}{d\Omega d\omega} = \frac{|e|^2}{16\pi^2 c} |g(\mathbf{k}, \tilde{\omega})|^2. \quad (4)$$

This can be written in terms of power as follows:

$$\frac{d^2 P(\tau)}{d\Omega d\omega} = \frac{|e|^2}{16\pi^2 c} \left[ \frac{dg(\mathbf{k}, \tilde{\omega})}{d\tau} g(\mathbf{k}, \tilde{\omega})^* + \text{c.c.} \right] \quad (5)$$

$$= \frac{|e|^2}{16\pi^2 c} \left[ g(\mathbf{k}, \tau) \int_{-\infty}^{\infty} d\tau' e^{i\tilde{\omega}(\tau - \tau')} g(\mathbf{k}, \tau') + \text{c.c.} \right], \quad (6)$$

$$\frac{d^2 P(\tau)}{d\Omega d\omega} = \frac{|e|^2}{8\pi^2 c} g(\mathbf{k}, \tau) \int_{-\infty}^{\infty} g(\mathbf{k}, \tau') \cos[\tilde{\omega}(\tau - \tau')] d\tau'. \quad (7)$$

Therefore the ‘‘electron injection function’’  $g(\mathbf{k}, \tau)$  will also be the temporal envelope of the emitted radiation. It describes where and when the electrons experience this violent acceleration to the speed of light. The dependence of the power spectrum on  $\tilde{\omega}$  and  $\mathbf{k}$  can obviously not be known without knowing the specific form of  $g(\mathbf{k}, \tau)$ .

The  $\mathbf{k}$  dependence should be broad due to the localization of the trapped electrons at the back of the wake. Similarly, simulations suggest that injection continues for hundreds of fs until beam loading prevents injection. This is in agreement with the temporal envelope for the injection seen in the experiment. The bandwidth generated by such a long temporal function would be too narrow to include the frequencies detected in the experiment. However, three-dimensional simulations and similarity theory [9] indicate small scale structure in the injected bunch. This would generate a white noise signal that is flat over a certain bandwidth. The structure is of the order of the laser frequency, and is thus consistent with the experimentally detected range of emission.

To estimate the expected energy radiated from this model, the function  $g(\mathbf{k}, \tau)$  can be assumed to be an incoherent series of microbunches with duration  $\tau_0$  and  $N_0$  electrons. Then the radiated energy emitted per microbunch would be (for a Gaussian temporal profile):

$$\frac{dE}{d\Omega} = \frac{|e|^2}{16\pi^2 c} N_0^2 \int e^{-(\tau_0^2 \omega^2/4)} d\omega. \quad (8)$$

If integrated between the experimental frequency limits for a bunch of  $10^6$  electrons and of  $\sim 1$  fs duration, then  $dE/d\Omega = 2 \times 10^{-12}$  J per bunch (between 0.1–3 fs yields the same result to within a factor of 2). For  $\sim 100$ 's of these microbunches adding incoherently the result is in reasonable agreement with the experimentally obtained value of  $10^{-10}$  J.

Numerical modeling of the experiment was performed in two dimensional slab geometry using the fully relativistic particle-in-cell code OSIRIS [18] on an eight node G5 cluster at Imperial College London. Fields in the code are handled by solving Maxwell's equations on a grid and hence should correctly model radiation generation by changing currents. To ensure that the radiation generated came from the electrons accelerated in the wakefield and not due to the interaction with the laser, the laser pulse was made shorter than in the experiment (15 fs). The radiation emitted from the interaction had its magnetic field component out of the slab. The laser field was polarized with magnetic field component in the slab so that the laser field could be completely decoupled from the radiation emitted by the electrons.

Figure 4 shows a two dimensional image of electron number density after the laser has propagated for 2.3 ps.

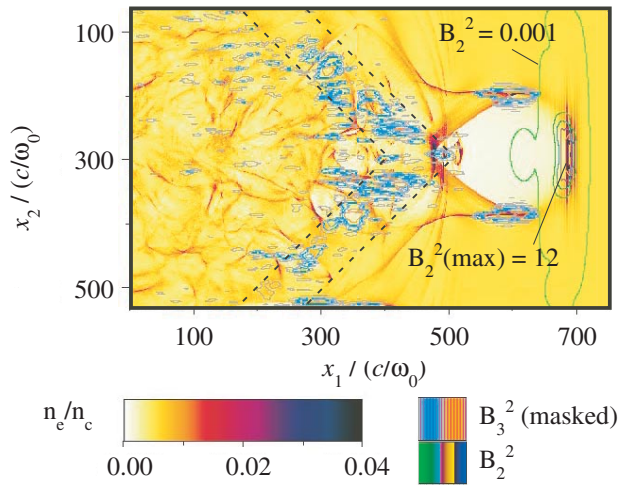


FIG. 4 (color). Simulated electron density  $n_e$  overlaid by contours showing the laser pulse magnetic field energy  $B_2^2$  (green) and the magnetic field energy of radiation emitted in the direction transverse to laser propagation  $B_3^2$  (blue).

Overlaid are contours of laser pulse magnetic field energy density ( $B_2^2$ , in green) and contours of transversely emitted magnetic field energy out of the slab ( $B_3^2$ , in blue). The components of  $B$  are normalized to  $m_e \omega_0 / e$ . The  $B_3$  component was Fourier filtered so that only  $\mathbf{k}$  vectors transverse to the laser propagation direction within an  $f/6$  cone, in the spectral range 300 nm to 1.1  $\mu\text{m}$ , are displayed. Radiation is seen to emanate from the region where the electron density and electric fields are highest, and slip back at  $45^\circ$ . As the simulation is in the wave frame,  $z - ct$ , this is equivalent to radiation propagating transverse to the laser direction in the lab frame.

Time histories of electron forward momentum and the spectrum of the magnetic field energy  $B_3^2$ , within the same cone and spectral range as above are shown in Fig. 5. There is a correlation between the onset of trapping and broadband spectral emission which switches off again when

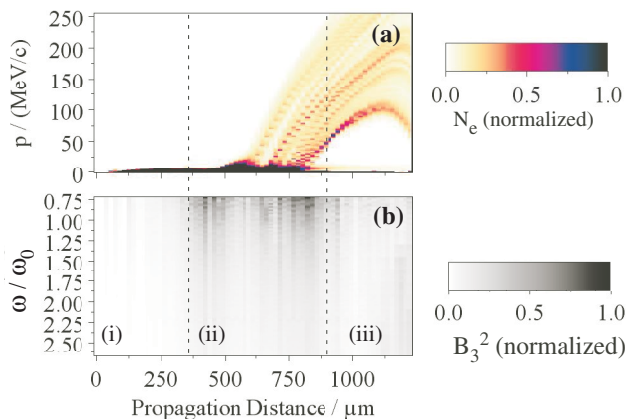


FIG. 5 (color). Time histories of (a) electron forward momentum and (b) spectrum of  $(B_3^2)_2$  in the simulation. Broadband emission correlates to injection of electrons.

beam-loading occurs. Figure 5 shows three distinct periods, (i), (ii), and (iii). In (i) the wake structure is developing and so no injection is occurring. In period (ii) the onset of trapping is observed [Fig. 5(a)], with a concurrent emission of broadband radiation [Fig. 5(b)]. Finally in (iii), even though the electron bunch is still experiencing a high rate of change of momentum, there is little radiation emitted. This is because the rate of change of velocity is again low.

In this Letter we have demonstrated the possibility of experimentally measuring the location of electron injection in an LWFA. Although the source is not very bright, the broadband nature of the radiation makes it easy to distinguish from other sources of radiation in the interaction. In addition to simply locating the point at which the injection occurs, the time for the laser pulse to evolve and the acceleration length can be known from the overall interaction length. This will provide a possible comparison between theory and experiment, and a useful diagnostic for future wakefield experiments.

This work was supported by EPSRC and the Alpha-X consortium. The authors acknowledge the staff of the Central Laser Facility for technical assistance. We gratefully acknowledge the OSIRIS consortium (UCLA/IST/USC) for the use of OSIRIS.

\*Present address: Institut für Optik und Quantenelektronik, Friedrich-Schiller-Universität, Max-Wien-Platz 1, 07743 Jena, Germany.

- [1] S. P. D. Mangles *et al.*, Nature (London) **431**, 535 (2004).
- [2] C. G. R. Geddes *et al.*, Nature (London) **431**, 538 (2004).
- [3] J. Faure *et al.*, Nature (London) **431**, 541 (2004).
- [4] T. Tajima and J. M. Dawson, Phys. Rev. Lett. **43**, 267 (1979).
- [5] A. I. Akhiezer and R. V. Polovin, JETP **3**, 696 (1956).
- [6] T. Katsouleas and W. B. Mori, Phys. Rev. Lett. **61**, 90 (1988).
- [7] A. Modena, Z. Najmudin, and A. E. Dangor *et al.*, Nature (London) **377**, 606 (1995).
- [8] S. V. Bulanov *et al.*, Phys. Rev. Lett. **78**, 4205 (1997).
- [9] S. Gordienko and A. Pukhov, Phys. Plasmas **12**, 043109 (2005).
- [10] F. S. Tsung *et al.*, Phys. Rev. Lett. **93**, 185002 (2004).
- [11] T. M. Antonsen and P. Mora, Phys. Fluids B **5**, 1440 (1993).
- [12] A. G. R. Thomas *et al.*, Phys. Rev. Lett. (to be published).
- [13] J. Faure *et al.*, Phys. Rev. Lett. **95**, 205003 (2005).
- [14] C. D. Murphy *et al.*, Phys. Plasmas **13**, 033108 (2006).
- [15] C. J. McKinstrie and R. Bingham, Phys. Fluids B **4**, 2626 (1992).
- [16] J. Schwinger, L. L. DeRaad, Jr., K. A. Milton, and W. Tsai, *Classical Electrodynamics* (Perseus Books, Cambridge, MA, 1998).
- [17] D. F. Gordon, B. Hafizi, R. F. Hubbard, and P. Sprangle, Phys. Plasmas **9**, 1157 (2002).
- [18] R. A. Fonseca *et al.*, in *Computational Science: Proceedings of ICCS 2002, Pt. III* (Springer-Verlag, Berlin, 2002), Vol. 2331, pp. 342–351.